# Synthesis and properties of Er³⁺-doped silica glass by sol-gel processing with organic complexation

XIUHONG HAN*, GUOZHONG CAO*, TOM PRATUM‡,
DANIEL T. SCHWARTZ§, BARRY LUTZ§
*Departments of* *Materials Science and Engineering,* ‡*Chemistry, and* §*Chemical
Engineering, University of Washington, Seattle, WA, 98195, USA*
*E-mail: gzcao@u.washington.edu*

Er³⁺-doped silica glass (up to 10 wt%) was synthesized by sol-gel processing with the addition of 3-aminopropyl trimethoxysilane (APS) as a complexing reagent. Er³⁺ ion reacted with the amino groups and, thus, linked to the silica network during the sol preparation. It is anticipated that the motion of Er³⁺ ions would be restricted, and the formation of Er³⁺ clusters inhibited. No detectable phase segregation was observed by means of SEM/TEM, regardless the addition of organic complexing reagent and heat-treatment. Nitrogen adsorption analysis indicated that dense glass was obtained after heating at 900–1000 °C for 10 hrs. Although the current experimental results were not conclusive, both fluorescence spectra and magic-angle spin (MAS) nuclear magnetic resonance (NMR) data were indicative that the addition of the complexing reagent APS might result in a homogeneous dispersion of high level Er³⁺ doping in the resultant gels. After the removal of organic components, however, Er³⁺ clustering occurs when firing at a high temperature for a long period of time, e.g. at 1000 °C for 10 hrs, due to enhanced Er³⁺ diffusion. © *2001 Kluwer Academic Publishers*

## 1. Introduction

Rare-earth (RE) -doped glasses are of great interest and have been investigated extensively and widely used in glass lasers [1, 2]. Silica glass is a highly attractive material as RE host matrix because silica glass has high glass transition temperature, low thermal expansion coefficient and low non-linear index of refraction [1]. Er³⁺-doped silica glass is of particular interest because the electronic transition of Er³⁺ from $^4I_{13/2}$ to $^4I_{15/2}$ emits light at a wavelength of 1.53 $\mu$m, which is outside the range of wavelengths focused on the retina of the human eye [3, 4], and is close to the wavelength of minimum loss window of silica glass [4–6]. This wavelength is used in the application of optical fibers and fiber amplifiers for optical communications [7]. In addition, Yb³⁺-codoped Er³⁺-doped silica glasses are used as active elements providing laser wavelengths in the blue and green regions [4, 8]. Er³⁺-doped silica fibers, fiber amplifiers and wave-guides have wide commercial uses due to their superior qualities. Optical fibers have demonstrated to be efficient with a low Er³⁺ doping [9]. For planar optical wave-guide amplifiers, however, due to a short optical interaction path, a high Er³⁺ doping concentration is needed to obtain sufficient optical amplification gains.

Despite about 20 years of extensive research, many challenges remain to be solved. For example, the molec- ular structure of the Er³⁺ environment in silica and the related fluorescence behavior is yet not well understood. Thermodynamically, RE have a low solubility in silica glass [1], and thus a doping concentration higher than the equilibrium solubility will lead to formation of RE clusters, which is detrimental to the optical properties of laser glasses. The formation of RE clusters results in fluorescence quench due to the interaction of neighboring RE ions. In traditional melt casting and chemical vapor deposition (CVD), the doping concentration is limited to the equilibrium solubility of RE ions in the host matrix [1]. To achieve a high doping level of RE ions in silica glass, a non-equilibrium low temperature approach is required to kinetically trap RE ions in host matrix with an atomic level homogeneity. Sol-gel processing is a suitable technique to achieve a high doping level of RE ions in silica glass with minimal formation of clusters of RE ions.

Although RE ion-doped sol-gel silica glass has a relatively large extent of homogeneous distribution of RE ions, it remains difficult to incorporate large quantities of RE ions into the rigid and covalently bonded tetrahedral $SiO_4$ glass network uniformly. Previous work has demonstrated that with a high doping concentration, RE (and other metals) ions have a strong tendency to form clusters in sol-gel silica as well [10–13]. At low concentrations, the RE ions can be distributed homogeneously

in a tetrahedral network with the formation of Si-O-RE structure. However, with an increasing concentration, due to strong interaction between the RE ions and oxygen ions, RE-O-RE clusters may form, and eventually lead to phase separation [14–16].

Several methods have been explored to improve the local environment of RE ions and to inhibit the formation of RE ion clusters during sol-gel processing, so as to prevent the fluorescence quench. The addition of certain codopants (such as a small quantity of $Al_2O_3$ or $P_2O_5$) into the glass network has been reported to spatially separate the RE ions [17]. The presence of codopants is speculated to partially or completely dissolve the clusters of RE ions in the host network resulting in a homogeneous distribution of RE ions in the silica glass structure even at high doping levels [17–19]. There are several reports about $Al^{3+}$ codoping effect in the matrix [4, 11, 20–26], including dispersion of $Al^{3+}$ codoped $Nd^{3+}$ [20–23], $Er^{3+}$ [4], and $Eu^{3+}$ [26] in sol-gel silica glasses. However, the introduction of codopant also results in an increased hydroxyl group content, which have an absorption band at $\sim 3470\,cm^{-1}$, resulting in hydroxyl quench. For example, the addition of $Al^{3+}$ and $Yb^{3+}$ as codopants to $Er^{3+}$-doped silica reduces the extent of clustering, but also leads to increased hydroxylation of RE ion and increased hydroxyl quench. The similar result was reported in the $Al^{3+}$ codoped $Eu^{3+}$-doped silica system [26, 27].

Introduction of organic components or modifying processing route has also been explored to incorporate RE ions into silica network homogeneously during sol-gel processing. Examples are a complexing reagent, such as N- (2-aminoethyl) -3-aminopropyl trimethoxysilane (DAMO) [28], a chelating ligands, such as (2, 6-pyridine dicarboxylic acid) [29] and weak (organic) acid salt [30] instead of mineral acid salts as source ions to introduce RE ions. As a high-field strength element, $Er^{3+}$ is likely to be a network former in a silica glass [31, 32]. Therefore, once $Er^{3+}$ forms chemical bonds with oxygen and thus links to the silica matrix, the kinetic rate of $Er^{3+}$ diffusion would be significantly reduced, even though the $Er^{3+}$ doping level in the silica matrix exceeds the thermodynamic equilibrium concentration. $Er^{3+}$ ions may be trapped kinetically in silica matrix and prevented from forming clusters, provided that prolonged heat-treatments at elevated temperatures are avoided. One of the key issues, therefore, is to control the process such that phase segregation will not occur before and during Er ions entering the silica matrix.

In this paper, we present a study on the synthesis of $Er^{3+}$-doped silica by sol-gel processing through organic ligand complexation. The objectives were to synthesize silica homogeneously doped with a high level of $Er^{3+}$ using organic complexing reagent (such as 3-aminopropyl trimethoxysilane (APS), $NH_2(CH_2)_3Si(OCH_3)_3$), by sol-gel processing and to understand the influences of the processing conditions and the addition of organic components on the local atomic environment. It is anticipated that APS plays a dual role in obtaining homogeneous distribution of $Er^{3+}$ ions in the silica network [28]: (1) to restrict the motion of $Er^{3+}$ ions in the resultant gels during process-

ing, aging and drying and (2) to incorporated $Er^{3+}$ into silica network through Si-O-Si linkage with the silica matrix originated from silica alkoxides. $Er^{3+}$-doped silica with and without APS was characterized by means of differential thermal and thermal gravimetric analyses (DTA/TGA), nitrogen adsorption, optical absorption spectrometry, Fourier transform infrared (FTIR), fluorescence spectrometry, and magic-angle spinning nuclear magnetic resonance (MAS-NMR). The content of hydroxyl groups (OH) in $Er^{3+}$-doped silica samples was quantified. The influences of organic complexing reagents and heat-treatment on the formation of $Er^{3+}$ clusters were discussed.

## 2. Sample preparation

All precursors and chemicals were used as received; no further treatment was conducted. Precursors and chemicals included tetraethoxysilane $Si(OC_2H_5)_4$ (TEOS, 99.99%, Aldrich, WI), hydrated erbium chloride ($ErCl_3 \cdot 6H_2O$, 99.99%, Alfa, MA), hydrochloric acid (1 N), D-I water, and 3-aminopropyl trimethylsilane $(CH_3O)_3Si(CH_2)_3NH_2$ (APS, 99.99%, Aldrich, WI). APS was used as complexing or coupling reagent.

Such unhydrolyzable organic ligand, which is attached to silicon through a metal-carbon bond, consists of an active group: $-NH_2$. The amino group is readily to react with and link $Er^{3+}$ to silica network and to immobilize $Er^{3+}$, so as to prevent the formation of $Er^{3+}$ clusters.

Fig. 1 is a flow chart of the sol-gel processing used to prepare $Er^{3+}$-doped silica samples. One set of samples had organic complexing reagent, and the other had no organic precursor. The doping concentration ranged from 0.01 wt% to 10 wt%. Silica sols were prepared by mixing TEOS and D-I $H_2O$ at room temperature under stirring at 250 rpm for 75 min. HCl was added as
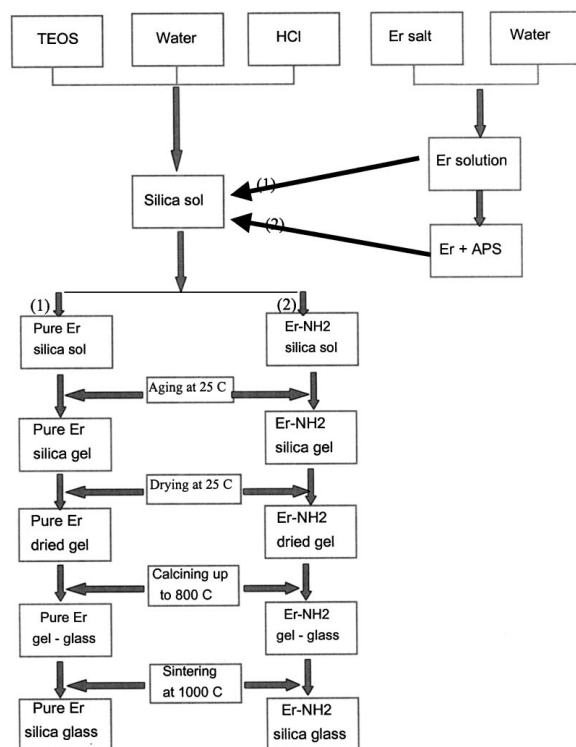


*Figure 1* Schematic flow chart of sample preparation procedure.

acid-catalyst to promote hydrolysis and condensation reactions, and the pH value of the sols were kept at approximately 1–2. The molar ratio of the sols were kept at $TEOS : H_2O : HCl = 1 : 14 : 0.1$.
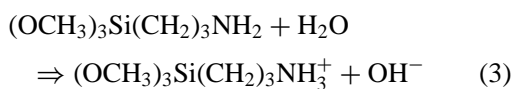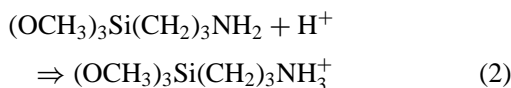
For $Er^{3+}$-doped silica sols without APS, $Er^{3+}$ aqueous solution was first prepared by dissolving $ErCl_3 \cdot 6H_2O$ into a small amount of D-I $H_2O$ and then admixed with the silica sol prepared as described above. The resulting $Er^{3+}$-doped silica sol had a pH value of 1.5–2.

$Er^{3+}$-doped silica sols with APS were prepared in a multi-step process. $ErCl_3 \cdot 6H_2O$ salt was first dissolved in a small volume of D-I water, then APS was added slowly to the $Er^{3+}$ aqueous solution under stirring at 250 rpm. The molar ratio of $ErCl_3 \cdot 6H_2O : APS$ was kept at 1 : 4. With the addition of APS, the $Er^{3+}$ aqueous solution first formed fine milky precipitates, and then the precipitates redissolved very quickly resulting in a clear stable solution. The addition of APS into the $Er^{3+}$ aqueous solution was proceeded further only after all precipitates were dissolved completely. The formation and dissolution of precipitates in preparation of $Er^{3+}$-APS solution might be attributed to the following:

APS reacted with $Er^{3+}$:

$$3(OCH_3)_3Si(CH_2)_3NH_2 + Er^{3+} \Rightarrow$$
$$((OCH_3)_3Si(CH_2)_3NH_2)_3 - Er^{3+} \qquad (1)$$
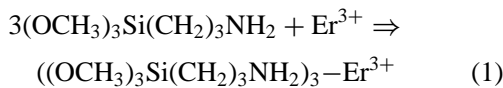
At the same time, APS might also react with $H^+$ ($pH < 7$) or $H_2O$ ($pH > 7$), when added into the $Er^{3+}$ aqueous solution:

$$(OCH_3)_3Si(CH_2)_3NH_2 + H^+$$
$$\Rightarrow (OCH_3)_3Si(CH_2)_3NH_3^+ \qquad (2)$$
$$(OCH_3)_3Si(CH_2)_3NH_2 + H_2O$$
$$\Rightarrow (OCH_3)_3Si(CH_2)_3NH_3^+ + OH^- \qquad (3)$$

When APS was added into the $Er^{3+}$ solution, reactions (2) and (3) might proceed very rapidly and result in a high pH in a local region. This high local pH value would result in the following reaction leading to the formation of $Er(OH)_3$ precipitates:

$$3OH^- + Er^{3+} \Rightarrow (Er(OH)_3) \downarrow \qquad (4)$$
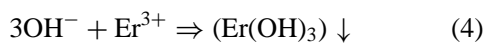
However, as reaction (1) proceeded and solution became more homogenously mixed, the reaction (4) would be reversed and the $Er(OH)_3$ precipitates dissolved quickly as the following reaction proceeded:

$$3(OCH_3)_3Si\text{-}(CH_2)_3NH_2 + Er(OH)_3 \downarrow \Rightarrow$$
$$((OCH_3)_3)Si\text{-}(CH_2)_3NH_2)_3 - Er^{3+} + 3OH^- \qquad (5)$$
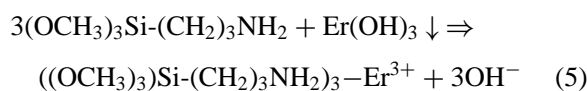
To verify the above hypothesis, the following experiment was conducted. 1 N $NH_4OH$ solution was added into the $Er^{3+}$ solution in exactly the same manner as APS. It was found that with the addition of $NH_4OH$ into $Er^{3+}$ aqueous solution, even the very first little drop of $NH_4OH$ solution led to irreversible precipitation, which never disappeared. The irreversible precipitation of $Er(OH)_3$ occurred when the pH value just reached about 4–5. The occurrence of $Er(OH)_3$ precipitates with the addition of ammonia solution is attributed to reaction (4). The above observations of the precipitation and dissolution of $Er(OH)_3$ with APS and irreversible precipitation with $NH_4OH$ imply that APS forms a complex with $Er^{3+}$ ions through the functional group, $-NH_2$. Since the molar ratio of $Er^{3+} : APS$ was kept at 1 : 4, if each $Er^{3+}$ ion formed complex with three APS, there would be one APS left over to react with $H^+$ or $H_2O$ (reaction (2) and (3)). As a result, the final pH value of the $Er^{3+}$-APS solution would be much higher than that of the initial solution. The increase in pH value was confirmed experimentally.

The resulting clear pink $Er^{3+}$-APS solution was then added dropwise into the silica sol. The addition of $Er^{3+}$-APS solution resulted in an appreciable increase in pH of the silica sol. 1 N HCl was added into the sol during the addition of the $Er^{3+}$-APS solution to adjust the pH value of the mixture solution and the pH was kept below 6, so as to prevent the formation of $Er(OH)_3$ precipitates. The pH value of the final $Er^{3+}$-APS silica sols varied $Er^{3+}$ concentration and ranged from 2 to 6.

Up completion of the sol preparation, the final sols were poured into petri dishes, sealed with parafilms, and allowed to gel at room temperature through further condensation. The gelation time ranged from an hour to approximately one month depending on the $Er^{3+}$ concentration, the presence of APS, and the pH value. For the samples prepared with APS, the gelation time is much shorter (typically about an hour) than that of the samples prepared without APS (typically a couple of weeks). The addition of APS resulted in a significant increase in pH value as described above. It is very well established that a higher pH value would result in a much shorter gelation time [33]. A higher pH value would also have a great influence on the final microstructure of the gels. The difference in microstructure of the initial solid gel network might also have some impacts on the microstructure local atomic environment and distribution of $Er^{3+}$ ions in densified silica glass as well. This will be discussed later in this paper. After gelation, wet gels were kept in sealed petri dishes for further aging for several weeks prior to drying. During drying, solvent was allowed to evaporate very slowly at room temperature through small holes punched on the parafilms. This drying process took several days before the parafilms were removed completely. The slow evaporation of solvent from wet gels minimized the drying stress gradient, and thus severe cracking was avoided and monolith $Er^{3+}$-doped silica gels were obtained. No macroscale precipitation or phase segregation was observed in all the samples by means of optical microscopy and scanning electron microscopy (SEM, Joel 52100).

Cracking was a common problem during drying and heating, and the thicker samples tended to crack severely. The propensity toward cracking was increased significantly with an increasing $Er^{3+}$ concentration and a decreasing pH value. The addition of APS has a significant influence on cracking as well. For the samples

with the same $Er^{3+}$ and APS concentrations but different pH values (e.g. one 1–2, another ~6), no appreciable difference was observed during drying. However, when heated at about 200°C, the sample with a low pH value became powder, while the sample with a high pH value remained intact. After drying, heat-treatment was conducted on $Er^{3+}$-doped silica gels to remove residual solvent, organic components and hydroxyl groups, and to densify the silica gel network. High resolution transmission electron microscopy (HR-TEM, Philips EM 430T) was applied to detect possible microscale phase segregation in $Er^{3+}$-doped silica samples. Thermal analysis was applied to analyze the removal of residual solvent, organic components and hydroxyl groups, while nitrogen adsorption was used to determine the pore volume.

## 3. TEM and thermal analysis

HR-TEM analysis revealed no detectable phase segregation in all $Er^{3+}$-doped silica gels or glass, regardless the addition of organic complexing reagent, prior to any heat-treatment or after full densification at 1000 °C for 10 hrs in air.

Thermal gravimetric analysis (TGA) and differential thermal analysis (DTA) were performed using NETZSCH STA/QMS system (NETZSCH Gerätebau GmbH). The typical amount of powder was approximately 300 mg. The heating rate was 3 °C/min and nitrogen or helium gas was used. TGA/DTA results of 10 wt% $Er^{3+}$-doped silica with and without APS indicate that a large exothermic peak accompanied by a drastic weight loss was observed at 120–150°C for both samples and can be attributed to the removal of residual solvent. Above 150°C, for $Er^{3+}$-doped silica without APS, TGA showed a gradual small weight loss. But for the sample with APS, there was a small exothermic peak at approximately 370°C accompanied with a significant weight loss, indicating the pyrolysis of the unhydrolyzable organic ligands of APS. During the heat treatment, the porous gels underwent de-hydroxylation or de-ethanolation (i.e. surface condensation), which resulted in a gradual weight loss as well as a decrease in pore volume or an increase in density. Such a surface condensation is a relatively slow and continuous process, which is in a very good agreement with the TGA result, i.e. a small but continuous weight loss as the heating temperature rises.

## 4. Pore volume analysis

Nitrogen absorption was used to determine the pore volume of $Er^{3+}$-doped silica glasses. The ambiently dried $Er^{3+}$-doped silica samples with and without the addition of APS were fired at 200°C, 400°C, 600°C, 800°C, and 1000°C for 10 hours in air with a heating rate of 1 °C/min. Samples were then ground to fine powders for nitrogen adsorption analysis using QUANTASORB (QUANTA CHROME, New York). Fig. 2 summarizes the pore volumes as a function of heating temperatures of silica doped with 10 wt% $Er_2O_3$ prepared with and without APS. One can see that there is a significant difference in the initial pore volumes of the samples prepared with and without APS. The samples made
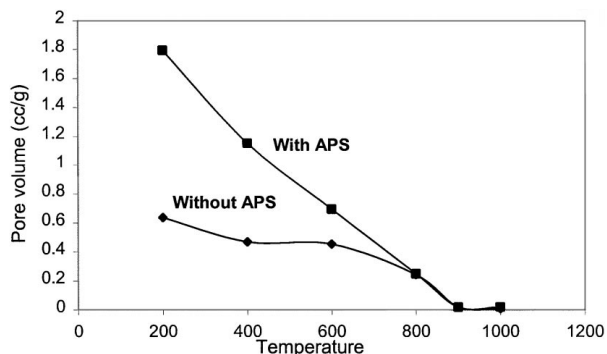


*Figure 2* Pore volume of 10 wt% $Er^{3+}$-doped silica (a) with APS and (b) without APS as a function of temperature (All samples were heat-treated at the given temperature for 10 hrs in air).

with APS possessed a significantly higher pore volume than the samples made without APS. This difference reduced gradually as the heating temperature rises, and diminished at 800°C. Almost dense glasses were obtained after heat-treated at 900 °C for 10 hours in air, regardless the initial pore volume.

The introduction of APS has an important impact on the evolution of silica gel network and the final microstructure of dried gels. The addition of APS resulted in a reduced connectivity of silica network, and thus led to a reduced mechanical strength, which led to the relatively easy formation of cracks upon the removal of pore fluid during drying and an increased extent of network collapse. On the other hand, the addition of APS resulted in an increase in pH from 2 to 6, and thus, greatly enhanced the condensation rate and significantly promoted the formation of three-dimensional clusters. As a result, a three-dimensional clustered network would retain a significantly porous structure. A significantly high porosity in $Er^{3+}$-doped silica with APS could be attributed to an increased pH value. In addition, a reduced capillary force, i.e. a reduced drying stress due to the hydrophobic organic ligands in APS might be contributed to the high porosity as well.

## 5. VIS absorption spectra measurements

VIS absorption spectra in the wavelength range of 380–780 nm were measured using spectrophotometer (American Laubscher Corp. NY). Tungsten lamp was used as VIS source and scan mode was used for the measurement. Fig. 3 is the absorption spectra of 10 wt% $Er^{3+}$-doped silica glass samples (a) without and (b) with addition of APS heat-treated at various temperatures in air for 10 hours. These spectra closely matched with the data reported in open literature [34, 35]. Several absorption peaks were observed from all the spectra, which are the characteristics of the typical atomic transition of $Er^{3+}$ ion in glassy matrix [24, 36] and their assignments are given in Table I. The peaks located at 488 nm, 525 nm, 550 nm and 660 nm represented the respective transitions from $^4I_{15/2}$ to $^4F_{7/2}$, $^2H_{11/2}$, $^4S_{3/2}$ and $^4F_{9/2}$. The intensities of all absorption bands increased with an increasing annealing temperature, suggesting that the local atomic environment of $Er^{3+}$ changed with thermal treatment, particularly, the removal of hydroxyl groups. The absorption spectrum

TABLE I Absorption peaks in the wavelength range 350–750 nm with assignments [1]

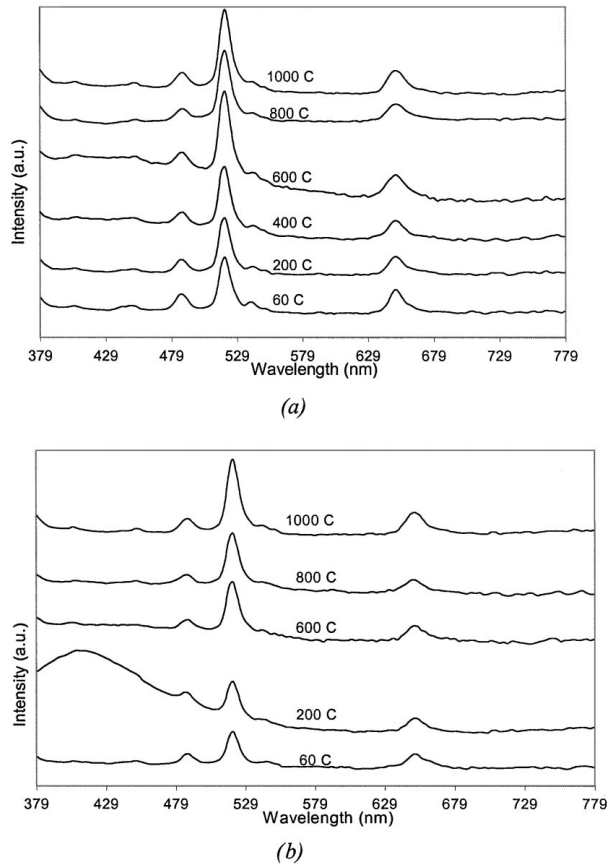| Peak wavelength (nm) | Assignment |
|---|---|
| 488 | $^4F_{7/2}$ |
| 525 | $^2H_{11/2}$ |
| 550 | $^4S_{3/2}$ |
| 660 | $^4F_{9/2}$ |

*(a)*



*(b)*

*Figure 3* Absorption spectra of (a) 10 wt% Er-doped silica without APS and (b) 10 wt% Er-doped silica with APS as a function of temperature.

of the sample with APS heat-treated at 200 °C shows a broad absorption band at 379–450 nm, which was attributed to the organic ligands of APS. The addition of APS had no influence on the positions and shapes of the bands. Optical microscope and Scanning electron microscope reveal that there was no observable inhomogeneity in all $Er^{3+}$-doped silica glass without or with heat-treatment up to 1000 °C. Absorption spectra of silica glasses with various $Er^{3+}$-doping concentrations were also measured. Identical absorption spectra were obtained and all absorption peaks of glasses have the same position and shape as that of 10 wt% $Er^{3+}$-doped silica glasses shown in Fig. 3. The absorption peak intensity increases with an increasing $Er^{3+}$ content.

## 6. $Er^{3+}$ fluorescence properties

The fluorescence spectrum in visible region was measured at room temperature with a home made Raman spectrophotometer, which has a resolution of 50 cm$^{-1}$. Argon laser with a wavelength 488 nm and a power

of 4 W was used to excite the sample. $Er^{3+}$ fluorescence spectrum around 1.5 $\mu$m was measured at room temperature with a 488-nm argon ion laser as an excitation source. The fluorescence signal was analyzed by a 48-cm monochromator in combination with a liquid-nitrogen-cooled Ge detector and recorded by a lock-in amplifier.

Fig. 4 shows the fluorscence spectra obtained from 10 wt% $Er^{3+}$ doped silica glass without APS and fired at various temperatures in air. The band at 595 nm in spectra of samples fired at low temperatures could be attributed to the residual organic components. Two fluorescence bands, centered at 550 and 670 nm, were observed in all spectra. According to the $Er^{3+}$ ion energy level diagram (Fig. 5), the emissions at 550 and 670 nm correspond to transitions from the $^4S_{3/2}$ and $^4F_{9/2}$ levels to the $^4I_{15/2}$ ground state, respectively. The fluorescence at 670 nm is most likely related to the clustering of $Er^{3+}$ in silica [37]. The population of electrons at $^4F_{9/2}$ level (670 nm) is due to a non-radiative transition from the $^4S_{3/2}$ level. $Er^{3+}$ clustering increases the probability of this transition [38], therefore, the electron
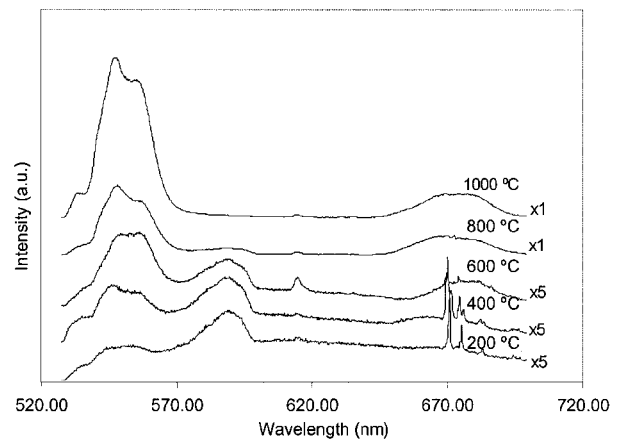


*Figure 4* Fluorescence spectra from the $Er^{3+}$ ion in 10 wt% sol-gel silica without APS and heat-treated at various temperatures in air. 488 nm argon laser was used as an excitation source.
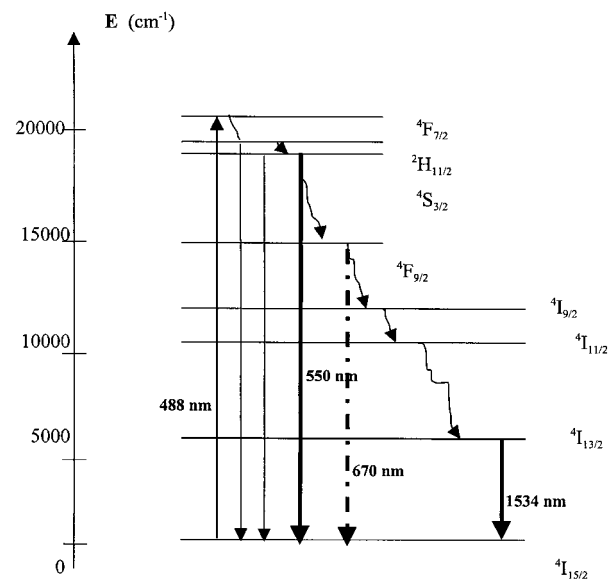


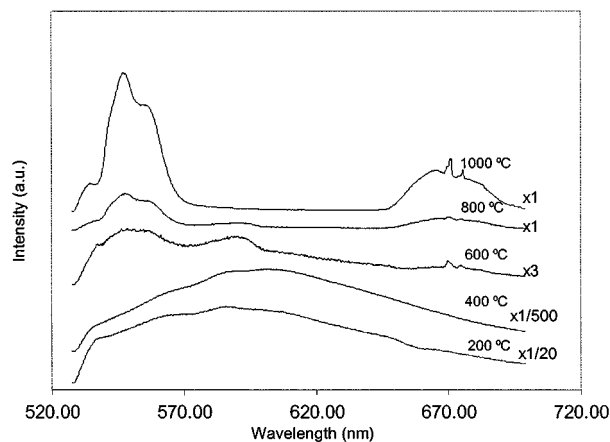*Figure 5* Energy levels of $Er^{3+}$ labeled with the dominant Russell-Saunder $^{2S+1}L_J$ term.

*Figure 6* Fluorescence spectra from the $Er^{3+}$ ion in 10 wt% sol-gel silica with APS and heat-treated at various temperatures in air. 488 nm argon laser was used as an excitation source.



*Figure 7* Fluorescence spectra from the $Er^{3+}$ ion in 10 wt% sol-gel silica with and without APS and heat-treated at 800 °C for 10 hrs in air. 514.5 nm argon laser was used as an excitation source.

population at the $^4F_{9/2}$ level increases significantly, resulting in an increased fluorescence emission at 670 nm. The appearance of strong fluorescence peak at 670 nm indicates the presence of $Er^{3+}$ in the high $Er^{3+}$-doped silica prepared without APS.

Fig. 6 shows the fluorescence spectra of 10 wt% Er-doped silica glasses with APS and fired at various temperatures in air. At temperatures below 800 °C, the spectra showed a very broad peak around 590 nm, due to the presence of organic components, and no fluorescence peak was observed, and there was also no detectable red emission band at 670 nm. As described above, this fluorescence band at 670 nm is related to clustering of $Er^{3+}$, and therefore, the absence of 670 nm fluorescence implies the absence or minimal presence of $Er^{3+}$ clustering. Although the exact mechanism is not known, a possible explanation is as follows. The incorporation of APS led to the formation of $Er^{3+}$-APS complex, which were homogeneously distributed in and linked to silica network during sol-gel processing, resulting in immobility of $Er^{3+}$ ions and prevention of $Er^{3+}$ clusters. This relatively homogeneous distribution of $Er^{3+}$ in silica network was retained after pyrolysis of APS at temperatures below 800 °C. After firing at a sufficiently high temperature, however, above 800 °C, $Er^{3+}$ ions gained a sufficiently high mobility and diffused through silica network, forming $Er^{3+}$ clusters.

Fig. 7 shows the fluorescence spectra of 10 wt% $Er^{3+}$-doped silica glasses with and without APS and heat-treated at 800 °C for 10 hrs in air. The fluorescence band at a wavelength 1.534 $\mu$m was observed for both samples, which corresponds to the transition from excited state $^4I_{13/2}$ to ground state $^4I_{15/2}$ as shown in Fig. 5. However, the full width of half maximum of the peak of the 10 wt% $Er^{3+}$-doped silica with APS is appreciably greater than that of the 10 wt% $Er^{3+}$-doped silica without APS, which implies more dispersed $Er^{3+}$ ions in silica network [4]. This is in a good agreement with fluorescence results in the visible region discussed above and the MAS-NMR results discussed below. It is also worth noting that the fluorescence intensity of 10 wt% $Er^{3+}$ doped silica with APS was found to be lower than that without APS. The reduced fluorescence intensity might be attributable to the relatively higher
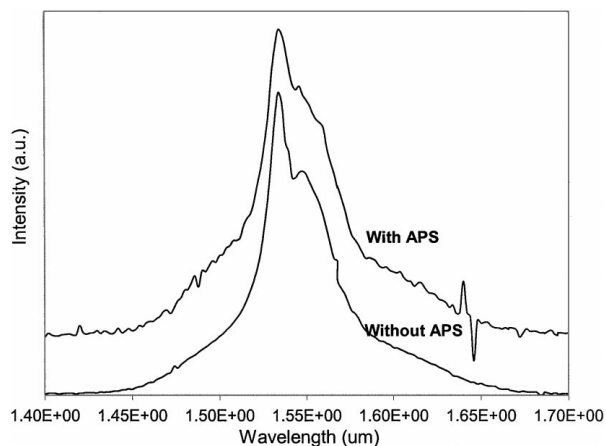
content of hydroxyl groups in the sample with APS, which will be discussed in detail in section VIII.

## 7. $^{29}$Si MAS – NMR spin – lattice relaxation study

$^{29}$Si (MAS)-NMR spin-lattice relaxation experiments were conducted on a modified Bruker AF300 FTNMR spectrometer operating at a frequency of 59.6 MHz for $^{29}$Si. Finely ground samples were put in a 7 nm $ZrO_2$ rotor spinning at 3.7–4.0 KHz in a Doty Scientific magic-angle spinning probe. In order to measure the $^{29}$Si spin-lattice relaxation time, $T_1$, a comb of twenty $\pi/2$ rf pulses was used to saturate the system and reduce the $^{29}$Si polarization to zero [39, 40]. The 90° pulse length for $^{29}$Si was 6 $\mu$s. After saturation, a free induction decay (FID) was recorded following a 90° observation pulse at various polarization recovery delay times (ranging from 10 to 500 s). The number of FIDs used to obtain $^{29}$Si spectrum varied from 96 for the longest delay time to 172 for the shortest delay time. Spectra were recorded at a similar signal to noise ratio.

It is known that $Er^{3+}$ ions form paramagnetic centers in silica glass [40]. Paramagnetic centers may contain just a single $Er^{3+}$ ion, or a cluster/group of $Er^{3+}$ ions in silica glass. When the paramagnetic centers are statistically randomly distributed and each $^{29}$Si nucleus relaxes only by its interaction with the surrounding paramagnetic centers (i.e. there is no spin diffusion which would result in $^{29}$Si relaxing one another), the relationship between the relaxation time, $T_1$, and the concentration of paramagnetic centers, $N_p$, will obey a scaling law [41]: $T_1 \propto N_p^{-4/3}$. Although the $^{29}$Si spin-lattice relaxation time can also be influenced by the electronic spin-lattice relaxation of the RE ions, this influence in $Er^{3+}$-doped silica system is negligible [40]. Therefore the $^{29}$Si relaxation time is considered to vary only with the concentration of paramagnetic centers, i.e., singly dispersed $Er^{3+}$ or clusters of $Er^{3+}$. If $Er^{3+}$ ions in silica were homogeneously dispersed at an atomic level, the concentration of paramagnetic centers would be equal to the concentration of $Er^{3+}$ ions. In this case, the relationship between the relaxation time $T_1$ and the
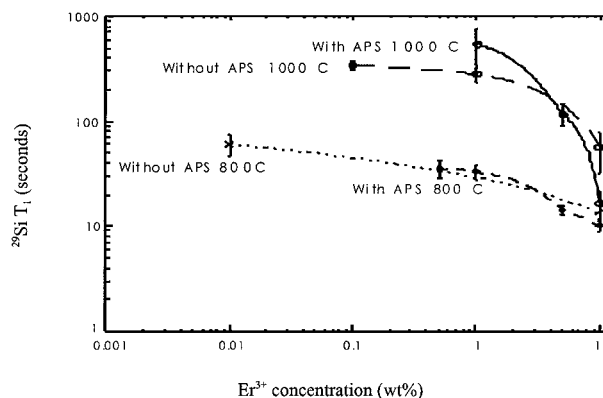
*Figure 8* The $^{29}$Si spin-lattice relaxation time as a function of the $Er^{3+}$ concentration in silica prepared with and without APS, (A) with APS heat-treated at 1000 °C for 10 hrs in air, (B) without APS heat-treated at 1000 °C for 10 hrs in air, (C) with APS heat-treated at 800 °C for 10 hrs in air, (D) without APS heat-treated at 800 °C for 10 hrs in air.

$Er^{3+}$ concentration, $[C_{Er3+}]$, would obey the scaling law: $T_1 \propto [C_{Er3+}]^{-4/3}$; when plotted double logarithmically, a slope of $-4/3$ should be obtained. However, if $Er^{3+}$ form clusters, the concentration of the paramagnetic centers would be less than the $Er^{3+}$ concentration introduced into silica. Consequently, the relationship between the relaxation time and the $Er^{3+}$ concentration will not follow this scaling law, and a longer relaxation time would be expected.

Fig. 8 shows the spin-lattice relaxation time ($T_1$) as a function of the $Er^{3+}$-doping concentration in $Er^{3+}$-doped silica with and without APS annealed at 1000 °C and 800 °C. Although the errors in the data are large, this figure shows the following: (1) the relaxation time decreases as the $Er^{3+}$ concentration increases, and (2) the addition of APS has distinct effects on the relaxation times of the samples heat-treated at 1000 °C with low and high $Er^{3+}$ doping concentrations. In particular, at the highest doping concentration, the addition of APS resulted in a reduced $^{29}$Si $T_1$, which was outside of experimental error at both 800 and 1000 °C heat-treated samples. According to the scaling law, a higher concentration of paramagnetic centers would result in a shorter relaxation time. This would imply that the samples with APS had a higher concentration of paramagnetic centers and therefore less clustering. However, the relationship between the relaxation time and the $Er^{3+}$ concentration in the samples prepared with APS annealed at 800 and 1000°C did not follow the scaling law. This is probably because some clustering occurred in all samples and the scaling law only applies to samples in which no clustering at all was present. Also, the relaxation time is not only dependent on the concentration of paramagnetic centers, but also highly sensitive to the local atomic structure. Since the preparation procedures were different for samples with APS from that without APS as described before, both the different preparation procedures and the addition of APS resulted in different initial microstructure. Such a difference may also have a great influence on the local atomic structure. Further detailed analysis on the local atomic structure is obviously needed. We also observed that the samples fired at 800 °C have a much shorter relaxation time than the corresponding samples fired at 1000 °C, regardless the $Er^{3+}$-doping concentration and the addition of APS. One possible explanation for this observation could be in terms of hydroxyl groups. Since protons also possess a relatively large nuclear magnetic moment, the interaction of this magnetic moment with nearby silicon nuclei can also act as a relaxation mechanism. This relaxation pathway would add to that already provided by the $Er^{3+}$, and observed $T_1$ could be greatly reduced. The FTIR data indicated that the concentration of hydroxyl groups in the samples annealed at 800 °C was much higher than that in the samples annealed at 1000 °C, especially for low concentration $Er^{3+}$-doped silica samples because the concentration of hydroxyl decreased with an increasing $Er^{3+}$ content. This large concentration of hydroxyl groups could have a significant influence on the spin-lattice relaxation of $^{29}$Si, and thus result in an increased relaxation rate.

## 8. Fourier transform infrared (FTIR) spectroscopy

The FTIR experiments were performed on a spectrometer (NICOLET Instrument Corp., WI) equipped with a CsI beam splitter and DTGS detector. 8 cm$^{-1}$ resolution and 40 scans were used and samples were prepared with the standard KBr pellet method, the ratio of KBr : sample = 200 mg : 1.2 mg.

Figs 9 and 10 show the evolution of IR transmission spectra of the 10 wt% Er-doped silica prepared with and without APS as a function of heat-treatment temperature. The assignments of IR absorption peaks are listed in Table II [28, 30, 44]. The large band between 3700 cm$^{-1}$ and 3200 cm$^{-1}$, is attributed to the O-H stretching vibration mode, and the intensity reduced as the heat-treated temperature rised. The presence of this O-H band remained up to 800 °C. Intensities of the Si-OH stretch band at 945 cm$^{-1}$ and H-O-H bending band at 1635 cm$^{-1}$ decreased as the heating temperature increased. Both stretch bands deminished when the samples were fired at 1000 °C. This could be explained by the surface condensation of silanol groups, which led to a decreased concentration of Si-OH and H-O-H and increased density. The nitrogen adsorption results described in section II clearly demonstrated that pore volume decreased with increased firing
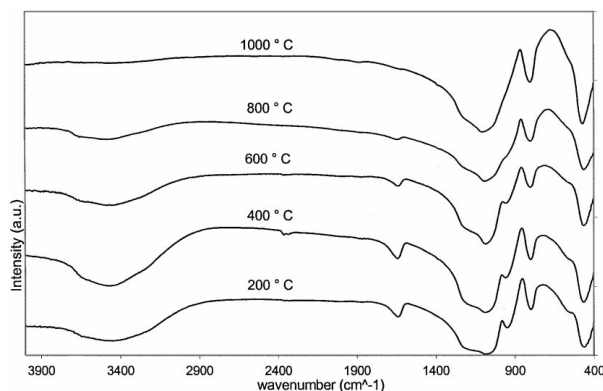


*Figure 9* Infrared transmission spectra of 10 wt% Er-doped silica without APS, and samples were heat-treated at various temperatures as indicated for 10 hrs in air.

TABLE II IR absorption peaks with assignments and relative intensities

| No. | Wave number (cm$^{-1}$) | Assignments | Intensity |
|---|---|---|---|
| 1 | 463 | O-Si-O bending vibration | Strong |
| 2 | 800 | Symmetric stretching of Si-O | Strong |
| 3 | 945 | Si-OH bending vibration | Strong |
| 3 | 1086 | Asymmetric stretching of Si-O | Strong |
| 4 | 1104 | Vibration of siloxane chains | Strong |
| 5 | 1580 | H-N-H bending vibration | weak |
| 5 | 1635 | H-O-H bending vibration | Strong |
| 5 | ~3470 | Si-OH stretching vibration | Broad and strong |

TABLE III OH concentrations change with different Er contents

| Er$_2$O$_3$ wt% | 0.1 wt% | 1.0 wt% | 5.0 wt% | 10 wt% |
|---|---|---|---|---|
| OH contents for sample without APS (ppm) | ~10200 | ~4900 | ~4400 | ~4300 |
| OH contents for sample with APS (ppm) | | ~4900 | ~4100 | ~3700 |



*Figure 11* OH contents of 10 wt% Er-doped silica with heat-treatment at various temperatures for 10 hrs in air.
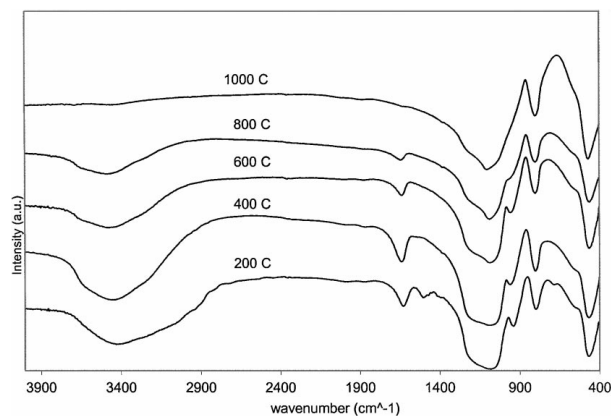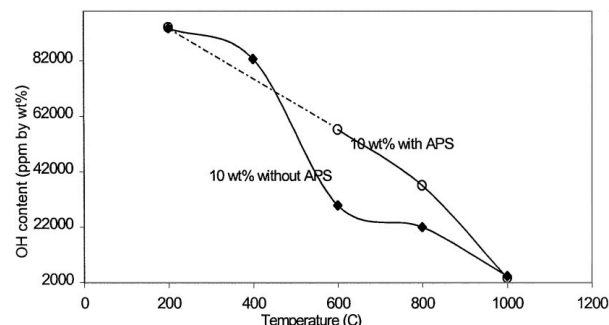


*Figure 10* Infrared transmission spectra of 10 wt% Er-doped silica with APS, and samples were heat-treated at various temperatures as indicated for 10 hrs in air.

temperature, and dense silica glass was obtained when fired at 1000 °C. A higher OH content in samples with APS could be contributed to a more porous structure (a higher pore volume, shown in Fig. 3), which in general is accompanied by a higher surface area. The bands 1086 cm$^{-1}$ (Si-O-Si asymmetric stretching), 797 cm$^{-1}$ (Si-O-Si symmetric stretching), and 463 cm$^{-1}$ (Si-O-Si bending) clearly observed in the spectra of the 600°C heat-treatment silica were shifted to 1106 cm$^{-1}$, 800 cm$^{-1}$, and 471 cm$^{-1}$ in the spectra of the 1000 °C heat-treatment glasses. The shift of the band positions is another proof of the full densification of the Er$^{3+}$-doped silica glass at 1000 °C [28, 45].

For silica glass as a host material, it is possible to quantitatively calculate the concentration of hydroxyl groups attached to the silica network as silanol ($\equiv$Si-OH) via the OH stretching band at around 3470 cm$^{-1}$ in the IR spectrum. The relationship between OH concentration and IR band intensity is given by the *Beer-Lambert law* [46]:

$$C = 10^6 \left[ MW \cdot \lg (T/T_0)/(\rho \cdot \varepsilon \cdot d) \right] \qquad (6)$$

Where $C$ is the concentration in ppm by weight, $MW$ is the molecular weight of the IR active component in g/mol, $T$ is the band intensity after going through samples in dimensionless transmittance units, $T_0$ is the band intensity before going through samples in dimensionless transmittance units, $\rho$ is sample density in g/L, $\varepsilon$ is the molar absorptivity or extinction coefficient of the

IR band in L/(mol.cm), and $d$ is the thickness of sample under the IR beam in cm.

Fig. 11 shows the OH contents as a function of firing temperatures calculated using Beer–Lambert equation. It is apparent that OH group content decreases as the heating temperature rises. The hydroxyl group content of the sample with APS heat-treated at 400 °C is not given in Fig. 11 since this sample became totally dark due to the incomplete prolysis of organic ligands. In general, the addition of APS resulted in a higher concentration of hydroxyl groups when heat-treated at low temperatures. This result might, at least in part, explain the relatively lower fluorescence intensity of the samples with APS (ref. Fig. 7). However, this difference disappeared when Er$^{3+}$-doped silica samples were heat-treated at temperatures higher than 800 °C. This observation may be attributed to the decrease in surface area. A high firinf temperature led to a lower pore volume (Fig. 2), which in general resulted in a low surface area. It was also found that the hydroxyl concentration decreased appreciably with an increasing content of Er$^{3+}$ ions in silica samples regardless of the addition of APS. The data in Table III summarizes the hydroxyl contents in silica samples heat-treated at 1000 °C, doped with various concentration of Er$^{3+}$. An increased Er$^{3+}$ concentration in silica was always accompanied in three times increase Cl$^-$ concentration, since ErCl$_3$6H$_2$O was used as the precursors. Both Cl$^{-1}$ and H$^+$ ions act as terminal ions in silica network and may form hydrochloric acid during heat-treatment. It is known that HCl effectively promotes dehydroxylation [47]. Another effect of an increased Er$^{3+}$ concentration is that a higher Er$^{3+}$ content on the surface would lead to a reduced content of silanol groups.

## 9. Conclusion
The addition of APS during sol-gel processing resulted in a significant increase in pH value and condensation rate, resulted in a much shorter gelation time. For a given Er$^{3+}$-doping concentration, the addition of APS

resulted in a much greater pore volume and hydroxyl group concentration. The differences in pore volume and hydroxyl group concentration decreased with an increased firing temperature and deminished when fired at 1000 °C for 10 hrs in air. Although both fluorescence spectra and MAS-NMR results are not conclusive, the fluorescence spectra implies that the clustering of $Er^{3+}$ in silica glass might be inhibited by the addition of APS during sol-gel processing. However, after the removal of complexing organic ligands and fired at high temperature such as 1000 °C, $Er^{3+}$ clusters formed due to enhanced diffusion of $Er^{3+}$ ions during heat-treatment at high temperatures. MAS-NMR data also imply that the addition of APS might result in an increasing concentration of paramagnetic centers, possibly indicating less $Er^{3+}$ clustering and a higher firing temperature led to more $Er^{3+}$ clusters. The addition of APS was found to result in an increased amount of hydroxyl groups. An approach to effectively densify $Er^{3+}$ and remove hydroxyl groups, but not significantly enhance the $Er^{3+}$ diffusivity is needed.

## Acknowledgment

## References

1. M. J. WEBER, *J. Non-Cryst. Solids* **123** (1990) 208.
2. J.-L. ADAM, J. LUCAS and S. JIANG, *SPIE* **2996** (1997) 8.
3. D. C. WINBURN, "Practical Laser Safety" (Dekker, New York 1985).
4. B. T. STONE and K. L. BRAY, *J. Non-Cryst. Solids* **197** (1996) 136.
5. A. POLMAN, *MRS Symp. Proc.* **316** (1994) 385.
6. T. MIYA, Y. TERUNUMA, T. HOSAKA and T. MIYASHITA, *Electronic Lett.* **15** (1979) 106.
7. B. J. AINSLIE, *J. Lightwave Tech.* **9** (199) 220.
8. J. L. JACKEL, A. YI-YAN, E. M. YOGEL, A. VON LEHMEN, J. J. JOHNSON and E. SNITZER, *Appl.-Opt.* **31** (1992) 3390.
9. N. KAGI, A. OYOBE and K. NAKAMURA, *IEEE Photo. Technol. Lett.* **2** (1990) 559.
10. N. I. KOSLOVA, B. VIANA and C. SANCHEZ, *J. Mater. Chem.* **3** (1993) 111.
11. I. THOMAS, S. PAYNE and G. D. WILKE, *J. Non-Cryst. Solids.* **152** (1992) 183.
12. L. LEE and D. TSAI, *J. Mater. Sci., Lett.* **13** (1994) 615.
13. W. V. MORESHEAD, J. R. NORGUES and R. H. KRABILL, *J. Non-Cryst. Soilds* **121** (1990) 267.
14. P. C. HESS, in "Physical Chemistry of Magmas, Advances in Physical Geochemistry," Vol 9, edited by L. L. Perchuk and I. Kushiro (Springer, New York, 1991) p. 152.
15. V. MCGAHAY and M. TOMOZAWA, *J. Non-Cryst. Solids* **159** (1995) 246.
16. J. WANG, W. S. BROCKLESBY, J. R. LINCOLN, J. E. TOWNSEND and D. N. PAYNE, *ibid.* **163** (1993) 261.
17. K. ARAI, H. NAMIKAWA, K. KUMATA, T. HONDA, I. YOSHIRO and T. HANDA, *J. Appl. Phys.* **59** (1986) 3430.
18. E. DELEVAQUE, T. GEORGES, M. MONERIE, P. LAMOULER and J.-F.-BAGON, *IEEE Photon, Technol. Lett.* **5** (1993) 73.
19. L. E. AGEEVA, V. I. ARBUZOV, E. I. GALANT, E. L. DEMSKAYA, A. K. PRZHEVUSKII and T. I. PROKHORAA, *Sov. J. Glass Phys. Chem.* **13** (1988) 221.
20. T. FUJIYAMA, T. YOKOYAMA, M. HORI and M. SASAKI, *J. Non-Cryst. Solids* **135** (1991) 198.
21. K. ARAI, H. NAMIKAWA, K. KUMATA and T. HONDA, *J. Appl. Phys.* **59** (1986) 3420.
22. K. ARAI, H. NAMIKAWA, Y. ISHII, H. IMAI and H. HOSONO, *J. Non-Cryst. Solids* **95/96** (1987) 609.
23. T. FUJIYAMA, M. HORI and M. SASAKI, *ibid.* **121** (1990) 272.
24. A. BISWAS, J. SAHU and H. N. ACHARYA, *Indian J. of App. Phys.* **34** (1996) 993.
25. B. T. STONE and K. L. BRAY, *MRS Symposium Proceedings* **435** (1996) 617.
26. M. J. LOCHHEAD and K. L. BRAY, *Chem. Mater.* **7** (1995) 572.
27. V. C. COSTA, M. J. LOCHHEAD and K. L. BRAY, *ibid.* **8** (1996) 783.
28. G. DE, A. LICCIULLI and M. NACUCCHI, *J. Non-Cryst. Solids* **201** (1996) 153.
29. D. C. LAI, B. DUNN and J. I. ZINK, *Inorg. Chem.* **35** (1996) 2152.
30. S. CHAKRABATTI, J. SAHU, M. CHAKRABORTY and H. N. ACHARYA, *J. Non-Cryst. Solids* **180** (1994) 96.
31. H. SCHOBE, "Glass" (Springer, New York, 1991) p. 136.
32. C. W. PONADER and G. E. BROWN JR., *Geochim. Cosmochim, Acta* **53** (1989) 2893.
33. C. J. BRINKER and G. W. SCHERER, "Sol-Gel Science" (Academic Press, San Diego, 1990).
34. K. SUN, W. H. LEE and W. M. RISEN. JR., *J. Non-Cryst. Solids* **92** (1987) 145.
35. D. MOUNTONNET, R. CHAPLAIN, M. GAUNEAU and Y. PELOUS, *Mater. Sci. Eng.* **B9** (1991) 455.
36. B. J. AINSLIE, S. P. CRAIG and S. T. DAVEY, *J. Lightwave Tech.* **6** (1988) 287.
37. K. KOJIMA, T. FUKUDA and M. YAMAZAKI, *Chemistry Letters* (1997) 931.
38. K. KOJIMA, S. YOSHIDA, H. SHIRAISHI and A. MAEGAWA, *Appl. Phys. Lett.* **67** (1995) 3423.
39. E. FUKUSHIMA and S. B. W. ROEDER, in "Experimental Pulse NMR: A Nuts and Bolts Approach" (Addison-Wesley, Boston, MA, 1981) p. 539.
40. S. SEN and J. F. STEBBINS, *J. Non-Cryst. Solids* **188** (1995) 54.
41. I. J. LOWE and D. TSE, *Phys. Rev.* **166** (1968) 279.
42. F. DEVREUX, J. P. BOILOT, F. CHAPUT and SAPOVAL, *Phys. Rev. Lett.* **65** (1990) 614.
43. W. E. BLUMBERG, *Phys. Rev.* **119** (1960) 79.
44. R. V. ADAMS and R. W. DOUGLAS, *Trans. Soc. Glass. Tech.* **XLIII** (1959) 147.
45. G. DE, D. KUNDU, B. KARMAKER and D. GANGULI, *J. Non-Cryst. Solids* **155** (1993) 253.
46. K. M. DAVIS, A. AGARWAL, M. TOMOZAWA and K. HIRAO, *ibid.* **203** (1996) 27.
47. F. KIRKBIR, H. MURATA, D. MEYERS, S. R. CHAUDHURI and A. SARKAR, *J. of Sol-Gel Sci. & Tech.* **6** (1996) 203.